Journal of Power Sources 196 (2011) 2979–2986

Contents lists available at ScienceDirect

Journal of Power Sources

journal homepage: www.elsevier.com/locate/jpowsour

Methanol electrooxidation at mesoporous Pt and Pt–Ru electrodes: A comparative study with carbon supported materials

Gonzalo García[a], Jonathan Florez-Montaño[a], Alberto Hernandez-Creus[a], Elena Pastor[a,*], Gabriel A. Planes[b,**]

[a] Departamento de Química Física, Instituto Universitario de Materiales y Nanotecnología, Universidad de La Laguna, Astrofísico F. Sánchez s/n, 38071 La Laguna, Tenerife, Spain
[b] Departamento de Química, Universidad Nacional de Río Cuarto, Agencia Postal 3, 5800 Río Cuarto, Argentina

ARTICLE INFO

Article history:
Received 1 August 2010
Received in revised form
27 September 2010
Accepted 7 November 2010
Available online 24 November 2010

Keywords:
Mesoporous materials
Micro fuel cells
PtRu
DEMS
Methanol electrooxidation
CO electrooxidation

ABSTRACT

The electrochemical behaviour of fuel cell catalysts (mesoporous Pt (MPPt), MPPtRu, MPPt modified by adsorbed Ru (MPPt/Ru) and carbon supported PtRu alloy) was studied using the thin layer flow cell differential electrochemical mass spectrometry (TLFC-DEMS) technique. The catalysts present high catalytic activity towards the methanol oxidation reaction (MOR), being the PtRu/C electrode the least active for MOR, while MPPt/Ru presents higher current densities for this reaction than MPPtRu. The results suggest that the diffusion properties obtained in the porous structure of the MP electrodes and the surface atomic arrangement in the electrode are the main reasons for the higher catalytic activity achieved. Finally, TLFC-DEMS was proved to be a powerful technique which evaluates and correlates the CO_2 efficiency with the catalytic activity and the porous structure of the catalysts.

1. Introduction

The employ of liquid fuel, such as methanol, as source of hydrogen offers some advantages respect to hydrogen fuel cell (PEMFC), especially on handling, storage, power density and transport [1]. These advantages allow the use of direct methanol fuel cell (DMFC) in portable electronic devices, but their performance is limited by several problems, like kinetic restraints, methanol cross-over from the anode to the cathode side through the membrane, and continuous poisoning of the catalysts due to the presence of intermediates generated in the methanol oxidation reaction (MOR) [1–3].

At present, PtRu catalysts are the most active for methanol oxidation [2]. Different electrode systems, such as electrochemical deposited Ru on Pt, bulk PtRu alloys and electrodeposited PtRu alloys, have been investigated extensively [4–9]. These studies have demonstrated that the presence of Ru on the electrode surface catalyses the oxidation of CO species, and consequently, enhances the electrocatalytic activity for methanol oxidation and other fuels.

Recently, the appearance of a new series of nanostructured metallic catalysts developed by soft templating has originated an attractive alternative to the traditional methods to obtain mesoporous (MP) electrodes. In this way, combining the soft template technique with electrochemistry is possible to obtain catalysts with high performance at the anodes and cathodes of fuel cells. These electrodes are especially interesting because they include in situ construction capabilities and accurate tailoring of the final porous structures [10,11]. In fact, during the last years the use of these MP materials as electrodes for methanol electrooxidation has been tested successfully [12–14].

On the other hand, Pt surface has been broadly modified by spontaneous deposition of metal adatoms (Pt/M) of diverse nature [15]. It was reported that Ru adatoms improve twice the catalytic activity against conventional PtRu alloys [16] during methanol electrooxidation. At the present, the catalytic activity of the catalysts has been attributed mainly to facts related to the chemical nature of the surface, such as improved water activation, appropriated crystallographic planes on metal surface, or parallel pathways [12,14,17,18].

Based on data provided by DEMS analysis, a new concept in the reaction mechanism of fuel cell catalysts was first proposed by Wang et al. [19,20] and later explored by Jusys et al. [21]. In this model, the fuel cell electrode can be considered as formed by a highly dispersed catalyst into a porous matrix, each active site may undergo to a particular condition for the access to reactants and products and sub-products release. Recently, we have studied the

* Corresponding author. Tel.: +34 922 319071; fax: +34 922 318002.
** Corresponding author: Tel.: +54 358 4676111; fax: +54 358 4676233.
E-mail addresses: epastor@ull.es (E. Pastor), gplanes@exa.unrc.edu.ar (G.A. Planes).

0378-7753/$ – see front matter © 2010 Elsevier B.V. All rights reserved.
doi:10.1016/j.jpowsour.2010.11.085

methanol oxidation on mesoporous Pt (MPPt) by thin layer flow cell differential electrochemical mass spectrometry (TLFC-DEMS) [14]. It was concluded that, under restricted diffusion of the soluble products (i.e. formic acid and formaldehyde), as occurs in real carbon supported catalysts, these products can readsorb and interact again with the catalytic surface, increasing the CO_2 efficiency. However, the current density diminishes.

In the present work we extend our previous analysis to more diverse systems in order to know the factors (i.e. geometry, chemical nature of the catalytic surface and support effect) that influence the observed electrode behaviour. In this way, diverse catalysts were studied, such as mesoporous electrodeposited Pt (MPPt), MPPt modified by adsorbed Ru (MPPt/Ru), MP coelectrodeposited Pt and Ru (MPPtRu) and carbon supported PtRu alloy (PtRu/C, 20 wt.% E-TEK). All of them were analysed towards CO and MOR by TLFC-DEMS at different temperatures. By means of quantitative DEMS analysis, the relationship between CO_2 yield and current density for all catalysts was evaluated. Additionally, the influence of the temperature, roughness factor, electrode materials and diffusion conditions for methanol oxidation was established.

2. Experimental

2.1. Electrode preparation

Mesoporous Pt electrodes were obtained by electrochemical reduction of a mixture of aqueous hexachloroplatinic acid (8%) and octaethyleneglycol monohexadecyl ether ($C_{16}EO_8$) (50% weight fraction) onto a DEMS Au disk electrode ($\varphi = 7$ mm) at 60 °C and 0.15 V. Typically, after 10 min of Pt^{4+} reduction, a charge of 749 mC cm^{-2} was passed during the deposition onto a Au substrate, resulting in a mesoporous Pt layer containing 1.04×10^{-4} g of Pt (assuming 75% efficiency). Then, the electrode was left in distilled water for 48 h, to let the surfactant be completely removed from porous structure. For MPPtRu electrodeposition, the aqueous fraction was composed of hexachloroplatinic acid (8%) and $RuCl_3$ in 1/1 metal ratio.

The surface modification by Ru adatoms was obtained in the following way: a MPPt electrode was immersed in 2 mM $RuCl_3$ + 0.1 M $HClO_4$ aged solution for 30 min with the purpose to facilitate the Ru dispersion inside the porous structure. After that, the electrode was rinsed with water, and finally transferred to an electrochemical cell containing 1 M $HClO_4$ (H_2SO_4 solution can not be used during this step due to interferences produced by sulphate co-adsorption). Finally, the electrode was cycled between 0.05 and 0.50 V to reduce the adsorbed Ru precursor to metallic Ru. The whole procedure was repeated three times.

In the studies of the carbon supported PtRu/C catalyst, the working electrode consists of a certain amount of the PtRu/C powder (20 wt.% metal supported on Vulcan XC-72, ETEK) deposited as a thin layer over a glassy carbon disc ($\phi = 7$ mm). For this purpose, an aqueous suspension of 4.0 mg ml^{-1} of the PtRu/C catalyst was prepared by ultrasonically dispersing it in 15 μl of Nafion (5 wt.% Aldrich) and pure water. An aliquot (20 μl) of the dispersed suspension was pipetted onto the glassy carbon surface and dried at ambient temperature under Ar atmosphere.

2.2. Physicochemical characterization

X-ray diffraction (XRD) patterns of the electrocatalysts were obtained using a universal diffractometer Carl Zeiss-Jena, URD-6, equipped with a Cu Kα radiation ($\lambda = 0.15406$ nm) generated at 45 kV and 40 mA. The real content of Pt and Pt–Ru in the electrocatalysts and the Pt to Ru ratio were determined by energy dispersive X-ray (EDX) technique coupled to a scanning electron microscopy Jeol JEMMod. 1010 with a silicon detector with Bewindowand applying 20 keV, while a scanning tunneling microscope (STM) from Nanoscope IIE, Digital Instrument was used to achieve surface images of the catalysts.

2.3. Electrochemical measurements

A high surface area carbon rod was used as a counter electrode and a reversible hydrogen electrode (RHE) in the supporting electrolyte was employed as reference electrode. All potentials in the text are referred to this electrode. Electrochemical measurements were performed with a computer-controlled HEKA potentiostat–galvanostat (PG 310). All experiments were carried out in a thermostatized electrochemical flow cell using a three-electrode configuration. The cell allows the exchange of the solution holding the potential control on the working electrode. Argon (N50) was used to deoxygenate all solutions and CO (N47) was employed for the adsorption experiences. Sulphuric acid and methanol (Merck, p.a.) were used for the preparation of the base electrolyte solution (1 M H_2SO_4) and methanol solution (1 M) in the base electrolyte.

In this work, currents are expressed as current densities J (A cm^{-2}), calculated from the measured current I (A) and the real electroactive area S (cm^2). S was estimated from the CO stripping from the relation $S = Q^{CO_2}/(n \times 210)$, where Q^{CO_2} is the charge obtained from the integration of the current recorded in the cyclic voltammogram for the stripping of CO_{ad} formed at $E_{ad} = 0.07$ V; n is the electrons exchanged in the oxidation reaction of CO to CO_2 ($n = 2$) and 210 μC cm^{-2} is the charge involved in a one electron per surface Pt atom reaction (linear configuration of adsorbed CO and full coverage are assumed).

2.4. TLFC-DEMS setup

This cell design permits the use of electrodes prepared by different methods under flow conditions (flow rate in the present communication: 0.4 ml min^{-1}). In addition, gaseous species produced on the electroactive surface can be followed on-line by mass spectrometry. Volatile species generated at the electrode evaporate at the pores of the membrane into the vacuum and are detected by the mass spectrometer with a time constant of ca. 1 s. This time constant is small enough to allow mass spectrometric cyclic voltammograms (MSCVs) for selected mass-to-charge ratios (m/z) to be recorded in parallel to cyclic voltammograms (CVs) at a scan rate of 0.02 V s^{-1}. A more detailed picture of the cell design is described in a previous communication [14].

2.5. TLFC-DEMS calibration

The calculation of the efficiency for methanol conversion to CO_2 by DEMS requires a previous determination of the m/z = 44 calibration constant (K^{CO_2}). This constant correlates the number of CO_2 molecules generated on the electrode surface (through the faradaic charge) with the portion of this molecules captured by the mass spectrometer (proportional to m/z = 44 ion current). K^{CO_2} has to be determined before each experiment because it depends of several variables (membrane–electrode gap, flow rate, temperature and pressure in the mass vacuum line) and it has to be fixed during the experience.

The calibration constant is calculated as follow: faradaic ($Q_f^{CO_2}$) and ionic m/z = 44 ($Q_i^{CO_2}$) charges were calculated from CO stripping and related according to equation:

$$K^{CO_2} = \left[2 \frac{Q_i^{CO_2}}{Q_f^{CO_2}} \right] \quad (1)$$

Then, the current efficiency E for methanol electrooxidation to CO_2 is determined from the subsequent equation:

$$E^{CO_2} = \frac{6Q_i^{CO_2}}{K^{CO_2}Q_f^T} \quad (2)$$

where Q_f^T is the charge associated to all faradaic processes occurring at the surface during methanol electroxidation (obtained from the cyclic voltammogram) and $Q_f^{CO_2}$ is the charge associated to the m/z = 44 signal recorded during the MOR.

3. Results

3.1. Mesoporous Pt production and characterization

The insert of Fig. 1 shows the current transient corresponding to the Pt salt reduction onto a Au electrode. Following an initial sharp peak due to the high Pt^{4+} abundances close to the electrode surface, a continuous decrease in the current was observed. A constant response was verified after a few seconds, in the mass transfer controlled region (see the double insert including the Cottrell representation).

Several potential cycles (not shown) between 0.05 and 0.90 V in acid media were required to clean the surface from residual adsorbed surfactant molecules. After that, the cyclic voltammograms for a MPPt electrode recorded at 0.20 V s^{-1} in 1 M H_2SO_4 (Fig. 1) shows neither residual current due to impurities nor diffusion complications.

At the macroscopic level, the surface looks as a smooth and shining metallic Pt layer. However, in the nanoscopic scale, the appearance is related to the quantity of catalyst deposited. At the initial stage, a uniform layer of metal characterized by small grooves produced by the liquid crystal patterning (Fig. 2A) is visible. Finally, metallic spheroids [22] are produced once the process begins to be controlled by diffusion (Fig. 2B). Note that the small metal clusters present in Fig. 2B are the initial stage for bigger nanospheres, visible at the image background.

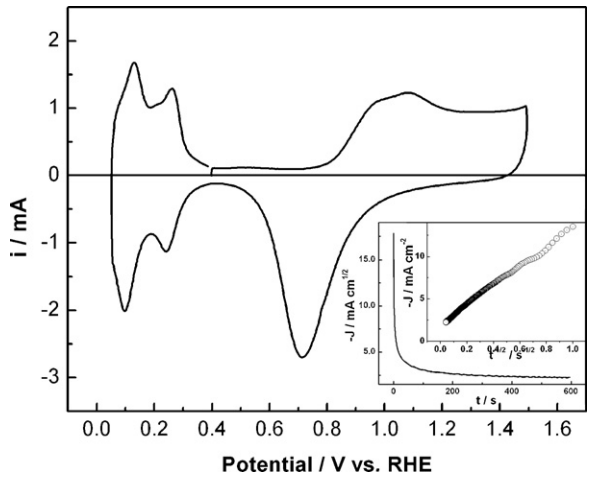

Fig. 1. Principal: Cyclic voltammogram for a MPPt electrode in 1 M H_2SO_4 at 0.2 V s^{-1}. Insert: Current transient during Pt deposition at 0.15 V_{RHE}. Double insert: Cottrell representation for the current recorded during Pt reduction at 60 °C.

The EDX analysis carried out over MPPt/Ru and MPPtRu samples shown compositions of 5% and 40% of Ru, respectively. However, it must be considered that the EDX sampling extends a few micro metre inside metal structure, where Ru is not present in the case of MPPt/Ru electrodes. This induces a sub-estimation of the Ru adatoms present at the surface of MPPt/Ru.

Fig. 3 shows the XRD patterns of the gold substrate as well as MPPt/Ru and MPPtRu electrocatalysts supported on gold. All the the sample show the typical peaks of the fcc structure of Pt (i.e. the planes (1 1 1), (2 0 0), (2 2 0), (3 1 1) and (2 2 2)) and those related to the gold substrate. These five peaks in the MPPtRu diffractogram are

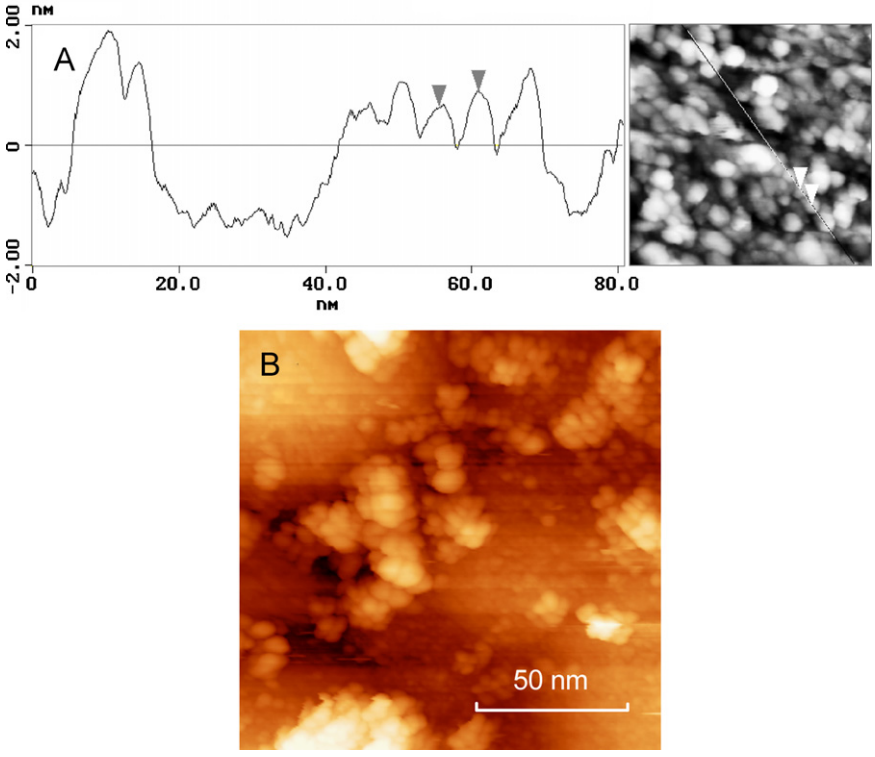

Fig. 2. (A) STM image (right) and the corresponding cross section analysis (left) at the initial stage of MPPtRu electrodeposition. (B) STM image of electrodeposited MPPt at the end of deposition (750 mC cm^{-2}). Nanoscope IIE, Digital Instrument.

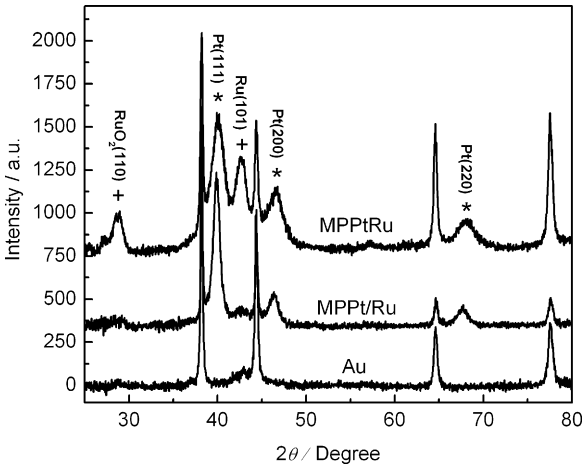

Fig. 3. XRD patterns of MPPt/Ru, MPPtRu and Au substrate samples. Main diffraction peaks related to Ru (+) and Pt (*) crystalline structure.

slightly shifted to higher angles with respect to the corresponding peaks in MPPt spectrum (not shown), indicating a small contraction of the lattice and possible alloy formation. Nevertheless, the MPPtRu electrode develops a large peak at ca. 42.7° related to the hexagonal structure of metallic Ru, while for the MPPt/Ru catalyst the same but smaller signal can be perceived. In addition, the MPPtRu material develops peaks at ca. 28° and 57° related to Ru oxides. Therefore, a metallic alloy formation is unlikely for MPPt/Ru due to the presence of pure metallic Ru and its oxides, but it cannot completely ruled out for MPPtRu.

3.2. CO electrooxidation

CO stripping experiments were performed in order to characterize the catalyst surface. The oxidation of a CO_{ad} monolayer gives useful information about the catalytic activity of the electrode and offers a safety way to estimate the final electroactive area before and after the surface modification with metallic adatoms (i.e. Ru).

Fig. 4 compares the stripping voltammetry observed for a CO saturated electrode for the three different catalysts (MPPtRu, MPPt/Ru and PtRu/C) at two temperatures (25 °C and 60 °C) at a scan rate of 20 mV s^{-1}. CO stripping voltammograms were obtained after bubbling CO through the cell for 10 min while keeping the electrode in the bulk of the solution at 0.07 V, followed by argon purging for 20 min to remove the excess of CO.

The CO stripping voltammograms depicted in the upper panel (Fig. 4A) were recorded with the MPPt/Ru surface. The modification of the MPPt surface with Ru atoms involved three exposition time of the electrode in the Ru solution followed by a stabilization procedure. After this procedure, the CO oxidation peak position shifts from 0.75 V_{RHE} at the MPPt electrode [14,23] to 0.56 V_{RHE} at the MPPt/Ru catalyst at 25 °C. A further exposition to Ru solution results in a displacement of the CO oxidation peak towards more positive potentials (not shown). A great shift to more negative potentials of the onset as well as the peak potential for the CO oxidation is observed with the increase of the temperature. In fact, the peak potential shifts from 0.55 V at 25 °C to 0.41 V at 60 °C, while the onset moves from 0.37 V at 25 °C to 0.23 V at 60 °C. Also, it is important to note the asymmetry of the peaks: they present a fast current increase followed by long current tail.

Fig. 4B shows the CO electrooxidation on the MPPtRu catalyst at two different temperatures. The peak potential decreases from 0.53 V at 25 °C to 0.43 V at 60 °C, while the onset moves from 0.36 V at 25 °C to 0.28 V at 60 °C. Interestingly, in this case the CO oxidation reaction presents a very symmetric peak at both temperatures.

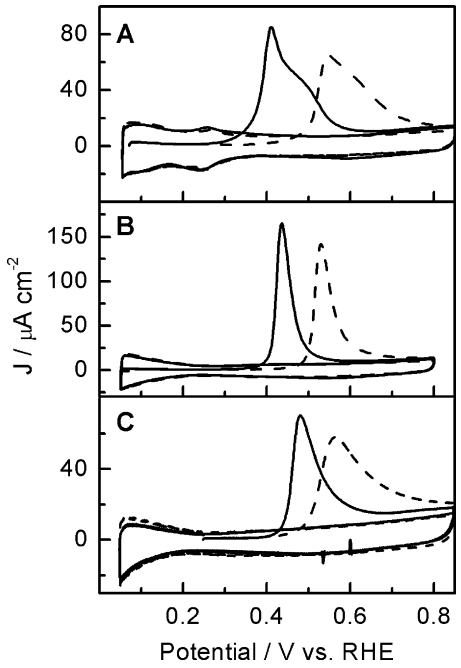

Fig. 4. CO stripping on MPPt/Ru (A), MPPtRu (B) and PtRu/C (C) electrodes. $\nu = 0.02$ V s^{-1}, 1 M H_2SO_4, 25 °C (– – – –) and 60 °C (—).

The lower panel of Fig. 4 displays the stripping voltammograms recorded with the commercial catalyst (PtRu/C) at the selected temperatures. The peak potential at 25 and 60 °C are located at 0.56 V_{RHE} and 0.48 V_{RHE} respectively; while no substantial dependence of the onset for the CO oxidation (~0.4 V_{RHE}) with temperature was observed for this catalyst. In addition, the shape of the CO oxidation peak turns to be more symmetric while the temperature increases.

In order to obtain more detailed information on the symmetry of the CO oxidation peak on the Pt catalysts, similar experiments were performed using perchloric acid. Fig. 5 compares CO stripping curves of MPPt/Ru recorded in 0.1 M $HClO_4$ with MPPt/Ru and MPPtRu in 0.1 M H_2SO_4 at 25 °C. It is remarkable the similarity of the CO stripping voltammograms for MPPt/Ru in 0.1 M $HClO_4$ and MPPtRu in 0.1 M H_2SO_4. The CO stripping voltammogram recorded with the catalyst modified with Ru on the surface presents a symmetric CO oxidation peak in perchloric acid (solid line) contrasting with the behaviour in sulphuric acid (dotted line). It is well known that sulphate adsorbs strongly on Pt surface [24], so the observed current tail in sulphuric acid has to be attributed to sulphate adsorption on the catalyst surface, which difficult the CO diffusion towards the most catalytic site. Interestingly, the MPPtRu catalyst (dashed line) seems to be not affected by sulphate species, pointing out the different surface structure obtained with diverse methodology (i.e. Ru adsorption and Ru co-deposition), which may affect any surface reaction. In fact, it is well know that metal oxides on the surface inhibit the adsorption of sulphate species [25] and it was proved by the XRD analysis that the MPPtRu electrode contains large amounts of Ru oxides.

3.3. Methanol electrooxidation

The electrode activity towards methanol electrooxidation was evaluated by cyclic voltammetry in 1 M CH_3OH + 1 M H_2SO_4 solution at 25 and 60 °C. The CVs (solid line) and the corresponding mass signals for CO_2 (m/z = 44) and formic acid (followed through methylformate formation, m/z = 60) during methanol electrooxidation at 25 °C can be seen in Fig. 6 for all MP electrodes. Also, it is

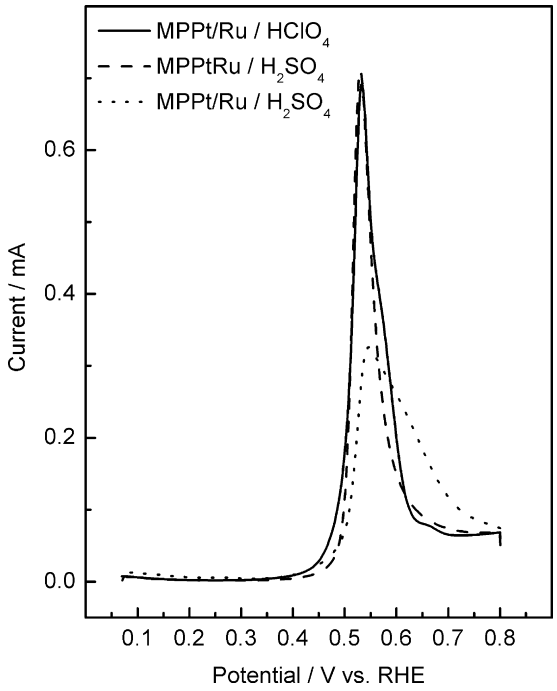

Fig. 5. CO stripping on MPPt/Ru (—) in 0.1 M $HClO_4$ and MPPt/Ru (. . .) and MPPtRu (– – – –) in 0.1 M H_2SO_4. $\nu = 0.02\ V\ s^{-1}$, 25 °C.

included the faradic current expected for 100% efficient conversion of methanol to CO_2 calculated from the m/z = 44 signals after the calibration procedure (dashed line). The difference in area between experimental (solid curve) and theoretical (dashed curve) currents is the extra charge associated with the formation of different products than CO_2 (formic acid can be indirectly detected by DEMS, but not formaldehyde). The presence of formic acid and its dependence with the applied potential can be visualized in the lower panel of Fig. 6.

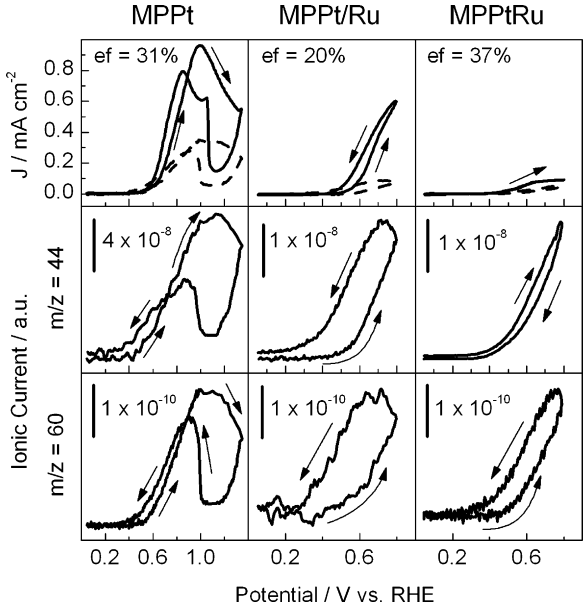

Fig. 6. CVs and MSCVs for CO_2 (m/z = 44) and HCO_2H (m/z = 60) formed during methanol electrooxidation on MPPt (left), MPPt/Ru (center) and MPPtRu (right). Faradaic current (—) and current calculated from CO_2 signal (m/z = 44) (– – – –). $\nu = 0.02\ V\ s^{-1}$, 1 M CH_3OH + 1 M H_2SO_4. $T = 25$ °C.

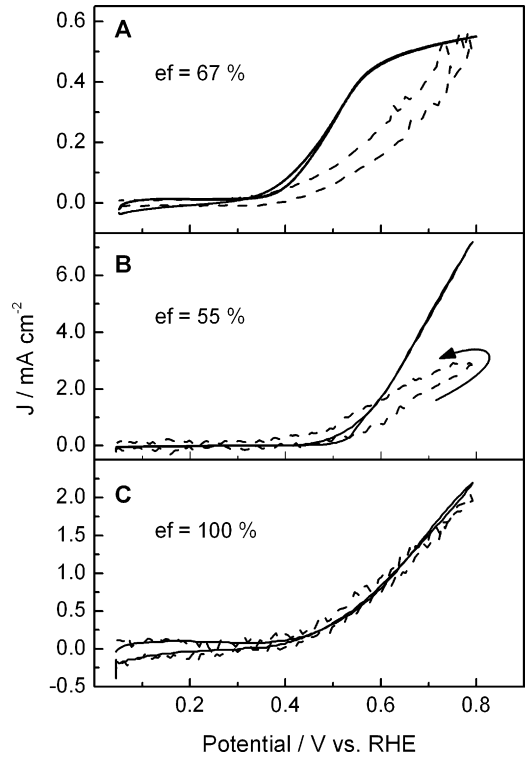

Fig. 7. CVs for (A) MPPtRu, (B) MPPt/Ru and (C) PtRu/C E-TEK. Faradaic current (—) and current calculated from CO_2 signal (m/z = 44) (– – – –). $\nu = 0.02\ V\ s^{-1}$, 1 M CH_3OH + 1 M H_2SO_4. $T = 60$ °C.

The same analysis has been carried out at 60 °C. Fig. 7 shows the CVs in 1 M CH_3OH + 1 M H_2SO_4 solution at 60 °C (solid line) and the faradic current expected for 100% efficient conversion of methanol to CO_2 calculated from the m/z = 44 signals (dashed line), for the MPPtRu and MPPt/Ru electrodes and the carbon supported PtRu (E-TEK) catalyst. The signals for the ionic masses are omitted for clarity.

A more reliable way to test the catalysts aptness for fuel cell applications involves chronoamperometric measurement of surface activity ($A\ cm^{-2}$) for methanol oxidation. The response of each electrode to a potential step from 0.05 V (a potential where methanol adsorption and oxidation are negligible) to 0.55 V (a potential similar to that achieved during operation conditions in a fuel cell) can be observed in Fig. 8. Commercial carbon supported PtRu catalyst was also tested for the sake of comparison.

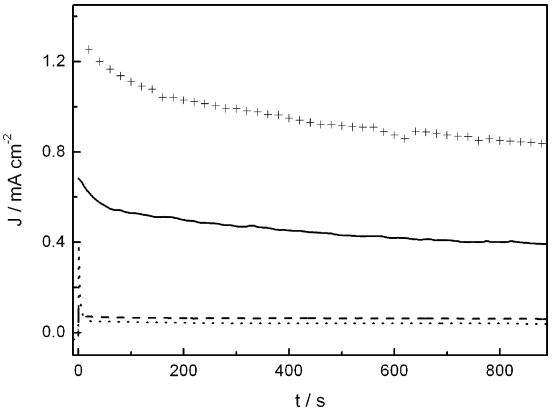

Fig. 8. Current transients for methanol electrooxidation on MPPt (. . .), MPPt/Ru (+++), MPPtRu (—) and PtRu/C E-TEK (– – – –) at 0.55 V_{RHE}. 1 M CH_3OH/1 M H_2SO_4. $T = 60$ °C.

4. Discussion

Fig. 4 shows the CO stripping experiences for each catalyst. The MPPt/Ru catalyst presents the best behaviour towards CO oxidation, with the lowest onset for CO oxidation at 0.23 V_{RHE} at 60 °C. This value is clearly more negative than the observed for the other catalysts at the same temperature. This material presents a noticeable shift in the peak potential for CO oxidation as result of Ru oxides formation at $E > 0.20\ V_{RHE}$. Consequently, the peak potential for CO_{ad} oxidation shifts to more negatives values for the Ru modified surface. Note that the onset for CO oxidation at MPPt/Ru electrodes at 25 °C occurs roughly at the same potential that the pre-peak observed during the CO oxidation at MPPt surface [14,23]. In addition, this electrode also shows an accentuated dependence of the onset for the CO oxidation reaction with the temperature, as well a marked broadening of the CO stripping peak after Ru deposition which was related to sulphate adsorption. The later is supported by previous investigations, in which similar electrochemical behaviour was observed with different Ru coverages (obtained by spontaneous deposition) on nanoparticles and smooth Pt [15,16]. However, for the extremely concave and irregular surface of MPPt (pore diameter ~3 nm) it is more difficult to extrapolate results. Due to the mesoporous morphology and small pore size, an accurate characterization of the Ru-modified MPPt will require a significant effort, and it will be the subject of further works.

On the other hand, the electrodeposition process used for MPPtRu synthesis seems to outcome in a more homogeneous metallic composition (bulk and surface), but with high Ru oxides coverage. Also, this surface presents an unique almost symmetric oxidation peak during CO stripping, which is characteristic of a fast CO diffusion on the surface towards the most active site. It is remarkable that the morphology of the MPPt/Ru and MPPtRu electrodes is similar but their metallic composition and atomic arrangement in the surface are totally different. Consequently, the catalytic activity towards the CO oxidation seems to be similar when the experiment is carried out in perchloric acid, but totally different when the effect of anion co-adsorption (i.e. sulphate species) is present. Once more, the difference during the CO oxidation in sulphuric acid between both Ru-based catalysts may be addressed principally to the presence of Ru oxides species on the MPPt/Ru surface.

In agreement with the literature [26,27], the CO stripping voltammogram recorded at carbon supported PtRu catalyst at 25 °C (Fig. 4C) presents a wide oxidation peak at 0.56 V_{RHE} with an onset located at ca. 0.38 V_{RHE}, in which its position is independent with the temperature.

In all cases, an increase of temperature result in a clear peak shift to more negative values, demonstrating an improved condition for CO elimination from the catalyst surface.

Fig. 6 compares the MOR for each electrode at 25 °C. It is evident that Ru modifies the electrode behaviour at $E < 0.6\ V_{RHE}$, where Pt–OH abundance at the surface is extremely low. The influence of the foreign metal (i.e. Ru) extends up to 0.7 V_{RHE}, where Ru-based catalysts show a near two-folded current density. At higher overpotenitials ($E > 0.75\ V_{RHE}$), the differences in catalytic activities descend due to the contribution of Pt–OH species to the bifunctional mechanism [8,28–30].

The CO_2 conversion efficiency (as average for a forward–backward scan) is in all cases lower than 40%, in agree with previous reported TLFC analysis for mesoporous catalysts [14]. The complete electrooxidation of methanol involves six electrons and gives CO_2 as final product. However, the low methanol conversion to CO_2 observed here involves the production of appreciable quantities of other reaction intermediates, such as formaldehyde and formic acid (Fig. 6C), which are formed in some fraction in the catalysts surface as consequence of partial alcohol oxidation (two and four electrons respectively).

The effect of increase the temperature reaction up to 60 °C (Fig. 7), results in a noticeable change of methanol conversion to CO_2 for all MP electrodes, reaching to 67% for the MPPtRu and 55% for the MPPt/Ru catalysts. Note, however, that CO_2 conversion for MP electrodes is far lower than verified for PtRu/C catalyst (100%). Additionally, PtRu/C shows the lowest surface activity (0.05 mA cm^{-2}) when it is compared with MPPtRu (0.38 mA cm^{-2}) and MPPt/Ru (0.42 mA cm^{-2}) at 0.55 V_{RHE}.

Fig. 8 shows the transients for methanol electrooxidation on all the catalysts at 0.55 V_{RHE}. It is remarkable that, considering the value of the stationary current, the catalytic activity for methanol oxidation at MPPt/Ru (0.82 mA cm^{-2}) is more than twice higher than the observed at MPPtRu catalyst (0.38 mA cm^{-2}). A two folded relationship in current density was reported by Waszczuk et al. [16] using nanoparticles as catalysts. They compared Pt nanoparticles decorated with ruthenium, and 1:1 PtRu alloy nanoparticles. We believe that the additional improvement observed in the present work could be related to the existence of especially active Ru surface states originated during Ru island formation [15] over an extremely curved surface, as was discussed above for the CO stripping, i.e. the morphology structure is similar in our MP electrodes but the distribution of the Ru atoms at the surface is different, which provides diverse properties such as stronger sulphate species adsorption and higher catalytic activity towards the MOR. Moreover, the difference in catalytic activity towards the methanol oxidation reaction may be related not only to Ru atomic distribution on the surface but also to the surface chemistry that is different for both Ru-based catalysts. It is well known that the presence of Pt and Ru oxides on the surface does not favour the dehydrogenation step[2].

In a general terms, the current density for MPPtRu (0.38 mA cm^{-2}) is in reasonable agree with that reported in ref [14] (~0.3 mA cm^{-2}), in particular considering that the synthesis parameters employed here, such as salts concentration, temperature and applied potential, are quite different. In the present work, the MP catalysts deposition occurs at higher overpotentials in the presence of low metal salt concentration. This combination produces high porosity and irregular surface (Fig. 2B). The latter is a relevant factor, because it generates a novel catalyst with a combined porous structure. The large gaps between the mesoporous Pt spheroids operate interconnecting all the MP structure, which turns into appropriates channels for mass transport inside the monolithic electrode. Even more, these gaps offers a suitable link between the inner and external surface.

However, the real dimension of the catalytic enhancement becomes clear when MPPt/Ru catalyst is compared with the carbon supported PtRu catalyst. The difference in the catalytic activity towards the methanol oxidation is more than one order of magnitude, being 0.82 mA cm^{-2} and 63 μA cm^{-2} for MPPt/Ru and PtRu/C, respectively (Fig. 8).

In order to check the proposed effect described in our previous report [14], in which the diffusion conditions are related to the catalytic activity, special care is necessary to prevent dissimilarity on catalysts load, especially for PtRu/C. For this reason a similar electroactive area and roughness factor are required for all catalysts, though the carbon supported catalyst seems to undergo restricted mass transport. In this context, the DEMS analyses depicted in the Figs. 6 and 7 support this idea, in which a real dependence between CO_2 production and electrode morphology is observed, being the diffusion of the intermediates (i.e. formic acid and formaldehyde) on the electrode surface the principal responsible for this fact. Moreover, this conclusion is supported by the

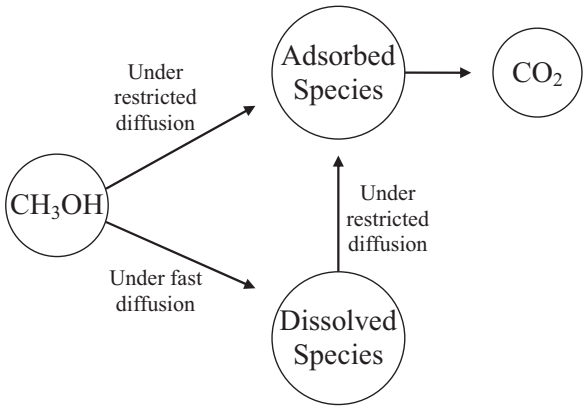

Scheme 1. Mechanism for methanol electrooxidation on mesoporous electrodes.

ratio between higher current densities with lower CO_2 conversion efficiency. It is clearly observable that MP catalysts develop higher current densities and lower efficiency for methanol conversion to CO_2 (~60%) than carbon supported Pt [14] and PtRu electrodes (~100%), in good agreement with our previous results [14]. Jusys et al. [21] found a similar effect on products distribution, keeping inalterable the inert porous matrix but offering more adsorption possibilities by increasing the metal load for carbon supported catalysts.

Scheme 1 depicts the proposed model for methanol electrooxidation. The production of CO_2 (and therefore the CO_2 efficiency) is related to the formation of adsorbed CO or other adsorbed species not detailed. Thus, an increase in CO_2 efficiency has to be accompanied by consumption of adsorbed intermediates (i.e. adsorbed CO). Then, under restricted diffusion, the soluble by-products (i.e. formaldehyde and formic acid) can interact again with the surface and readsorb. As a consequence, the amount of adsorbed CO increases during the complete oxidation process, and accordingly, the CO_2 efficiency. However, the current density diminishes.

Moreover, the restricted diffusion emphasizes the competitive effects for reactions sites onto inner porous surface between methanol molecules and partially oxidized by-products. Finally, it is observed that electrodes with restricted diffusion increase the relative quantities of formic acid and formaldehyde due to the difficulty of these molecules to leave out of the porous structure, obstructing in this way the free pore-replenishment by methanol.

5. Conclusions

Complete procedures to obtain MPPtRu and MPPt/Ru catalysts were developed. The electrodes obtained in this way have shown to be highly efficient for methanol oxidation. The least active catalyst for methanol oxidation is the PtRu/C electrode, while the unsupported MPPt/Ru catalyst is more active than the MPPtRu one.

It was observed that an electrode properly structured and modified, such as a monolithic catalyst electrode, can offers better performance towards methanol electrooxidation than a traditional carbon supported catalysts which have higher specific areas.

Results can be understood taking into account the especially accessible porous structure of mesoporous electrodes produced by electrochemical reduction under mass transfer controlled regimen. In the resulting structure, the possibility of readsorption of partially oxidized products is low. As a consequence, the surface coverage by adsorbed CO decreases and the turnover frequency increases during methanol oxidation. The high current developed at mesoporous catalysts during the methanol oxidation is originated in a first stage by a fast CO elimination due principally by the second metal (i.e. Ru) which provides sites that promotes the OH formation at more negative potentials than Pt. After that, the reaction is mainly enhanced by the existence of alternative paths for methanol electrooxidation to formic acid and formaldehyde, which do not involves the formation of adsorbed CO. In addition, it was observed a better performance for the MPPt/Ru than the MPPtRu towards the methanol oxidation, which was suggested to be due to a surface factor: absence of Ru oxides and a better surface atomic arrangement on the MPPt/Ru surface.

TLFC-DEMS has demonstrated to be an appropriate technique for the determination of reaction products during methanol electrooxidation at MP and carbon supported catalysts. With the aid of DEMS calibration, it is possible to evaluate the efficiency for CO_2 conversion and correlate it with the porous characteristics of the catalyst.

The results obtained in the present work support the idea that the porous architecture is an important factor for the observed electrode behaviour. This factor is crucial and has a relative importance comparable to the chemical nature of the surface. Due to the high porosity of real fuel cell electrodes, results in the present paper can be of importance for the application of the developed materials in this type of systems. Consequently, further works in the field are necessary.

Catalysts easily produced as MPPtRu and MPPt/Ru electrodes have good possibilities to be used in special applications (i.e. micro fuel cells), where high catalysts surface load and scale factors make the in situ construction an essential issue [31].

Acknowledgments

Authors thank the MICINN for financial support (project MAT2008-06631-C03-02) and the AECID for sustaining the cooperation between both universities (PCI A/025292/09). J.F. acknowledges ACIISI (Gobierno de Canarias) for the predoctoral fellowship.

References

[1] X. Ren, P. Zelenay, S. Thomas, J. Davey, S. Gottesfeld, J. Power Sources 86 (2000) 111.
[2] A.S. Aricò, S. Srinivasan, V. Antonucci, Fuel Cells 1 (2001) 133.
[3] B. Gurau, E.S. Smotkin, J. Power Sources 112 (2002) 3339.
[4] G. García, J.A. Silva-Chong, O. Guillén-Villafuerte, J.L. Rodríguez, E.R. González, E. Pastor, Catal. Today 116 (2006) 415.
[5] G. García, V. Baglio, A. Stassi, E. Pastor, V. Antonucci, A.S. Aricò, J. Solid State Electrochem. 11 (2007) 1229.
[6] C.E. Lee, S.H. Bergens, J. Phys. Chem. B 102 (1998) 193.
[7] W.F. Lin, M.S. Zei, M. Eiswirth, G. Erh, T. Iwasita, W. Vielstich, J. Phys. Chem. 103 (1999) 6968.
[8] H.A. Gasteiger, N. Markovic, P.N. Ross Jr., E. Cairns, J. Phys. Chem. 98 (1994) 617.
[9] Z. Jusys, H. Massong, H. Baltruschat, J. Electrochem. Soc. 146 (1999) 1093.
[10] G.S. Attard, P.N. Bartlett, N.R.B. Coleman, J.M. Elliot, J.R. Owen, J.H. Wang, Science 278 (1997) 838.
[11] J.M. Elliot, G.S. Attard, P.N. Bartlett, N.R.B. Coleman, P.A.S. Merckel, J.R. Owen, Chem. Mater. 11 (1999) 3602.
[12] J. Jiang, A. Kucernak, J. Electroanal. Chem. 533 (2002) 153.
[13] J. Jiang, A. Kucernak, Chem. Eng. J 93 (2003) 81.
[14] G.A. Planes, G. García, E. Pastor, Electrochem. Commun. 9 (2007) 839.
[15] A. Crown, C. Johnston, A. Wieckowski, Surf. Sci. 506 (2002) L268.
[16] P. Waszczuk, J. Solla-Gullón, H.S. Kim, Y.Y. Tong, V. Montiel, A. Aldaz, A. Wieckowski, J. Catal. 203 (2001) 1.
[17] A. Rodes, J. Clavilier, J.M. Orts, J.M. Feliu, A. Aldaz, J. Electroanal. Chem. 338 (1–2) (1992) 317.
[18] M.T.M. Koper, J. Electroanal. Chem. 574 (2) (2005) 375.
[19] H. Wang, C. Wingender, H. Baltruschat, M. Lopez, M.T. Reetz, J. Electroanal. Chem. 509 (2001) 163.
[20] H. Wang, T. Loffler, H. Baltruschat, J. Appl. Electrochem. 31 (7) (2001) 759.
[21] Z. Jusys, J. Kaiser, R.J. Behm, Langmuir 19 (2003) 6759.
[22] J. Jiang, A. Kucernak, Chem. Mater. 16 (2004) 1362.
[23] G. García, M.M. Bruno, G.A. Planes, J.L. Rodriguez, C.A. Barbero, E. Pastor, Phys. Chem. Chem. Phys. 10 (2008) 6677.
[24] A. Kolics, A. Wieckowski, J. Phys. Chem. B 105 (2001) 2588.

[25] F.C. Nart, T. Iwasita, J. Electroanal. Chem. 308 (1991) 277.
[26] Z. Jusys, T.J. Schmidt, L. Dubau, K. Lasch, L. Jörissen, J. Garche, R.J. Behm, J. Power Sources 105 (2002) 297.
[27] S. Pasupathil, V. Tricoli, J. Solid State Electrochem. 12 (2008) 1093.
[28] C. Roth, A.J. Papworth, I. Hussain, R.J. Nichols, D.J. Schiffrin, J. Electroanal. Chem. 581 (2005) 79.
[29] L.L. Mickelson, C. Friesen, J. Am. Chem. Soc. 131 (2009) 14879.
[30] M. Watanabe, S. Motoo, J. Electroanal. Chem. 60 (1975) 267.
[31] Toshiba at the CeBIT Electronics Fair in Hanover, August 2003.